THE JOURNAL OF BIOLOGICAL CHEMISTRY VOL. 287, NO. 53, pp. 44062–44070, December 28, 2012

A Na^+/Ca^{2+} Exchanger-like Protein (AtNCL) Involved in Salt Stress in *Arabidopsis*[*S]

Received for publication, February 9, 2012, and in revised form, November 7, 2012 Published, JBC Papers in Press, November 12, 2012, DOI 10.1074/jbc.M112.351643

Peng Wang[‡1], **Zhaowei Li**[‡§1], **Jingshuang Wei**[¶], **Zenglin Zhao**[‡], **Daye Sun**[‡], **and Sujuan Cui**[‡2]

From the [‡]*Hebei Key Laboratory of Molecular Cell Biology, College of Life Science, Hebei Normal University, Shijiazhuang 050024, China, the* [§]*College of Biological Science and Engineering, Hebei University of Science and Technology, Shijiazhuang 050018, Hebei, China, and the* [¶]*New Drug R&D Center, State Key Laboratory of Development of Antibody Drugs, North China Pharmaceutical Group Corporation, Shijiazhuang 050015, China*

Background: Na^+/Ca^{2+} exchangers were found in animals, but no Na^+/Ca^{2+} exchanger had been reported in plants.
Results: AtNCL showed Na^+/Ca^{2+} exchanger-like activity and regulated stress response.
Conclusion: Functional Na^+/Ca^{2+} exchanger-like protein exists in plants.
Significance: Na^+/Ca^{2+} exchange also play a role in Ca^{2+} homeostasis under abiotic stress in plants.

Calcium ions (Ca^{2+}) play a crucial role in many key physiological processes; thus, the maintenance of Ca^{2+} homeostasis is of primary importance. Na^+/Ca^{2+} exchangers (NCXs) play an important role in Ca^{2+} homeostasis in animal excitable cells. Bioinformatic analysis of the *Arabidopsis* genome suggested the existence of a putative NCX gene, *Arabidopsis NCX-like* (*AtNCL*), encoding a protein with an NCX-like structure and different from Ca^{2+}/H^+ exchangers and Na^+/H^+ exchangers previously identified in plant. AtNCL was identified to localize in the *Arabidopsis* cell membrane fraction, have the ability of binding Ca^{2+}, and possess NCX-like activity in a heterologous expression system of cultured mammalian CHO-K1 cells. *AtNCL* is broadly expressed in *Arabidopsis*, and abiotic stresses stimulated its transcript expression. Loss-of-function *atncl* mutants were less sensitive to salt stress than wild-type or *AtNCL* transgenic overexpression lines. In addition, the total calcium content in whole *atncl* mutant seedlings was higher than that in wild type by atomic absorption spectroscopy. The level of free Ca^{2+} in the cytosol and Ca^{2+} flux at the root tips of *atncl* mutant plants, as detected using transgenic aequorin and a scanning ion-selective electrode, required a longer recovery time following NaCl stress compared with that in wild type. All of these data suggest that *AtNCL* encodes a Na^+/Ca^{2+} exchanger-like protein that participates in the maintenance of Ca^{2+} homeostasis in *Arabidopsis*. AtNCL may represent a new type of Ca^{2+} transporter in higher plants.

Calcium ions (Ca^{2+}) are required for many physiological functions. Numerous stimulations produce change in the cytosolic concentration of Ca^{2+} $[Ca^{2+}]_{cyt}$[3] (1–11). The mechanisms of production and elimination of $[Ca^{2+}]_{cyt}$ have become a key topic in Ca^{2+} signaling and related functions. Various environmental stresses can stimulate the opening of Ca^{2+}-permeable channels in the plasma or inner membrane, leading to an influx of Ca^{2+} along its electrochemical gradient (12, 13). After this influx, the cytosolic level of Ca^{2+} could be returned to its resting state through the activity of several types of Ca^{2+} transport proteins that extrude Ca^{2+} out of the cytosol.

In animal cells, Ca^{2+} transport proteins include Ca^{2+}-ATPase pumps that use ATP directly and transporters that are driven indirectly by ATP using ion gradients (14–19). Na^+/Ca^{2+} exchangers (NCXs) are due to the later Ca^{2+} transport proteins. Na^+/Ca^{2+} exchange was first reported in guinea pig cardiac muscle (20). Since then, NCX proteins have been identified in the plasma membrane of many types of cells (21–27). NCX proteins, which consist of 9–11 transmembrane domains with a large intracellular hydrophilic loop, play important roles in adjusting the $[Ca^{2+}]_{cyt}$ (28). For example, NCXs maintain the $[Ca^{2+}]_{cyt}$ during the intrinsic excitation-contraction cycle in cardiac muscle cells (29). NCXs are bidirectional Ca^{2+} transporters, and the direction of Ca^{2+} flux is dependent on the electrochemical Na^+ gradient (30–33). Thus, NCXs play important roles in Ca^{2+} signaling and homeostasis in animal cells.

Until recently, only Ca^{2+}/H^+ exchangers (CAXs) and Ca^{2+}-ATPases were reported to transport Ca^{2+} through the membrane in plant cells (1,34–39), whereas Na^+/H^+ exchangers (NHXs) were reported to drive Na^+ through the plasma membrane based on a H^+ gradient (40, 41). Thus, we sought to address whether a protein similar to animal NCXs exists *in planta*. Wang *et al.* suggested the existence of Na^+-dependent Ca^{2+} uptake activity in vacuolar membrane vesicles from wheat(42). Here one NCX-like gene in Arabidopsis (*AtNCL*)

* This work was supported by National Basic Research Program of China Grant 2006CB100101 and Research Program of the Ministry of Agriculture, China, Grant 2008ZX08009-003 (to D. S.); National Science Foundation of Hebei Province, China, Grant C2009001516, New Century Excellent Teacher Project of Education Department, China, Grant NCET-06-0256, and National Basic Research Program of China Grant 2006CB910600 (to S. C.).
[S] This article contains supplemental Figs. S1–S6, Table S1, and additional references.
[1] Both authors contributed equally to this work.
[2] To whom correspondence should be addressed. Tel.: 86-311-80787535; Fax: 86-311-80787535; E-mail: cuisujuan@mail.hebtu.edu.cn.

[3] The abbreviations used are: $[Ca^{2+}]_{cyt}$, cytosolic Ca^{2+} concentration; AAS, atomic absorption spectroscopy; ABA, abscissic acid; AtNCL, *Arapidopsis* NCX-like; CaBD, Ca^{2+} binding domain; CaM, calmodulin; CAX, cation/Ca^{2+} exchangers; GUS, β-glucuronidase; NCX, sodium/calcium exchanger; NHX, sodium/proton exchanger; PI, propidium iodide; qRT-PCR, quantitative RT-PCR; SIET, scanning ion-selective electrode technique.

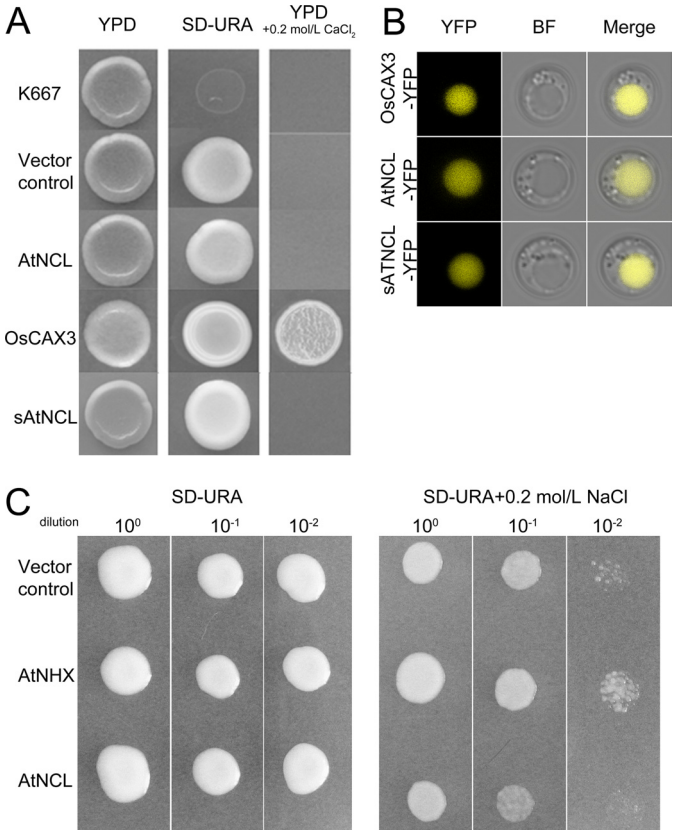

FIGURE 1. **AtNCL shows no CAX/NHX-like activity in yeast.** *A*, the expression of *AtNCL* and *sAtNCL* in K667 mutant yeast did not complement the Ca^{2+}-hypersenstive phenotype. OsCAX3 was used as a positive control. *B*, the localization of AtNCL-YFP, sAtNCL-YFP, and OsCAX3-YFP in K667 cells was similar. *YFP*, YFP channel; *BF*, bright field channel; *Merge*, merged image of the YFP and BF channels. *C*, the expression of *AtNCL* in AXT3 mutant yeast did not complement the Na^+-hypersensitive phenotype.

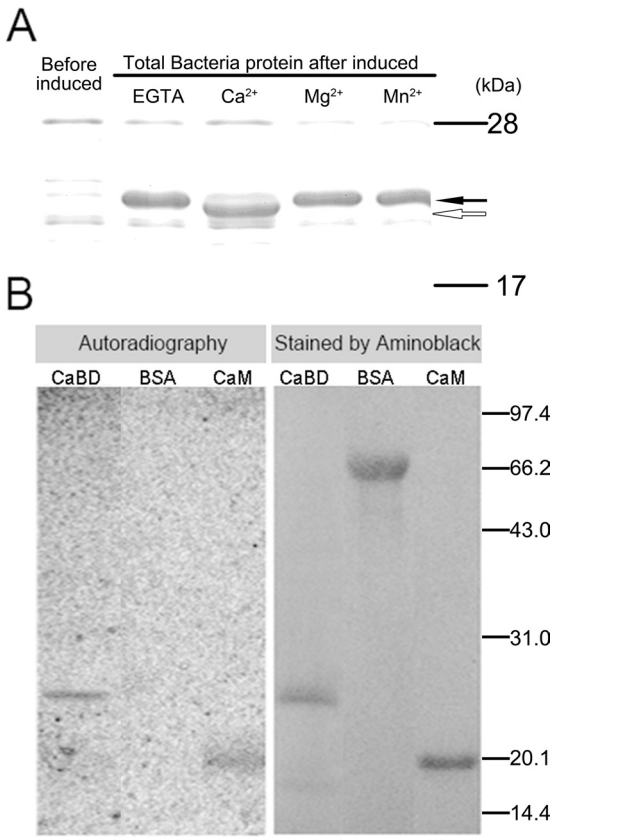

FIGURE 2. **The putative EF-hand domains of AtNCL can bind Ca^{2+}.** *A*, Ca^{2+}-dependent electrophoretic mobility shift of the recombinant putative CaBD. EGTA, Mn^{2+}, Ca^{2+}, or Mg^{2+} was added at a final concentration of 5 mM to the bacterial proteins dissolved in 18% SDS-PAGE sample buffer. The *hollow arrow* indicates the CaBD band in the presence of Ca^{2+}, which ran faster than in the presence of EGTA, Mn^{2+}, or Mg^{2+} (*filled arrow*). *B*, purified CaBD, BSA, and CaM were separated by 12% SDS-PAGE and transferred to PVDF membranes for a $^{45}Ca^{2+}$ binding assay and Amido Black staining. The molecular masses of the standards in kDa are shown at the *right* of the sections.

encoded a protein similar to animal NCXs in structure, had Na^+/Ca^{2+} exchange activity, and was involved in Ca^{2+} homeostasis under salt stress in *Arabidopsis*.

EXPERIMENTAL PROCEDURES

Plant Materials and Growth Conditions—The *Arabidopsis thaliana* stocks described in this work were of the Columbia (Col) ecotype. *atncl-1* and *atncl-2* correspond to Syngenta Arabidopsis Insertion Library (SAIL)_791_D12 and SAIL_770_A10, respectively. For salt stress, 7-day-old seedlings were transferred to plates containing 1/2 MS medium or 1/2 MS medium supplemented with 150 mM NaCl. After 7 days, the seedlings were photographed, and the survival rate was determined based on the number of plants with two to four true leaves that had become completely white in color; the chlorophyll content was measured as reported previously (43). Freezing tolerance was assayed as described (44), 10-day-old seedlings were frozen at −6 °C for 3 h and thawed at 4 °C for 12 h. After a 5-day recovery, survival rate and chlorophyll contents were measured. Heat stress was performed as described previously (45). 7-day-old seedlings were exposed to 45 °C for 75 min and recovered at 22 °C for 7days.

Yeast Functional Complementation Test—A CAX function test was carried out in *Saccharomyces cerevisiae* strain K667 (*MATa cnb1::LEU1 pmc1::TRP1 vcx1*Δ) as described (36). The coding sequences of AtNCL, sAtNCL, and OsCAX3 were isolated and cloned into p416GPD then transformed into K667 cells using the LiAc/PEG method. Saturated liquid cultures of K667 containing the various plasmids were diluted to A_{600} = 1.0 then spotted onto selection medium (-Ura), yeast extract peptone dextrose (YPD) medium, or YPD containing 200 mM $CaCl_2$. The dishes were incubated at 30 °C for 3 days before taking pictures.

NHX function test was carried out in *S. cerevisiae* strain AXT3 (Δ*ena1–4::HIS3,* Δ*nha1::LEU2,* Δ*nhx1::TRP1*) (46). AtNCL and AtNHX1 (46) were cloned into pDR195 and transformed into AXT3 cells. Cells were cultured in selection medium (-Ura). Saturated liquid cultures were diluted and spotted onto selection medium (-Ura, 20 g/liter galactose, 20 g/liter agar) with or without 200 mM NaCl. The dishes were incubated at 30 °C for 4 days before taking pictures.

Quantitative RT-PCR— qRT-PCR was employed to measure the transcript levels. The RNA samples were pretreated extensively with an RNase-free DNase to remove any contaminating genomic DNA prior to use. The PCR primers are listed in supplemental Table 1. qRT-PCRs were performed in 96-well blocks with an Applied Biosystems 7500 real-time PCR system using the SYBR Green I mix in a volume of 20 μl. The specificity

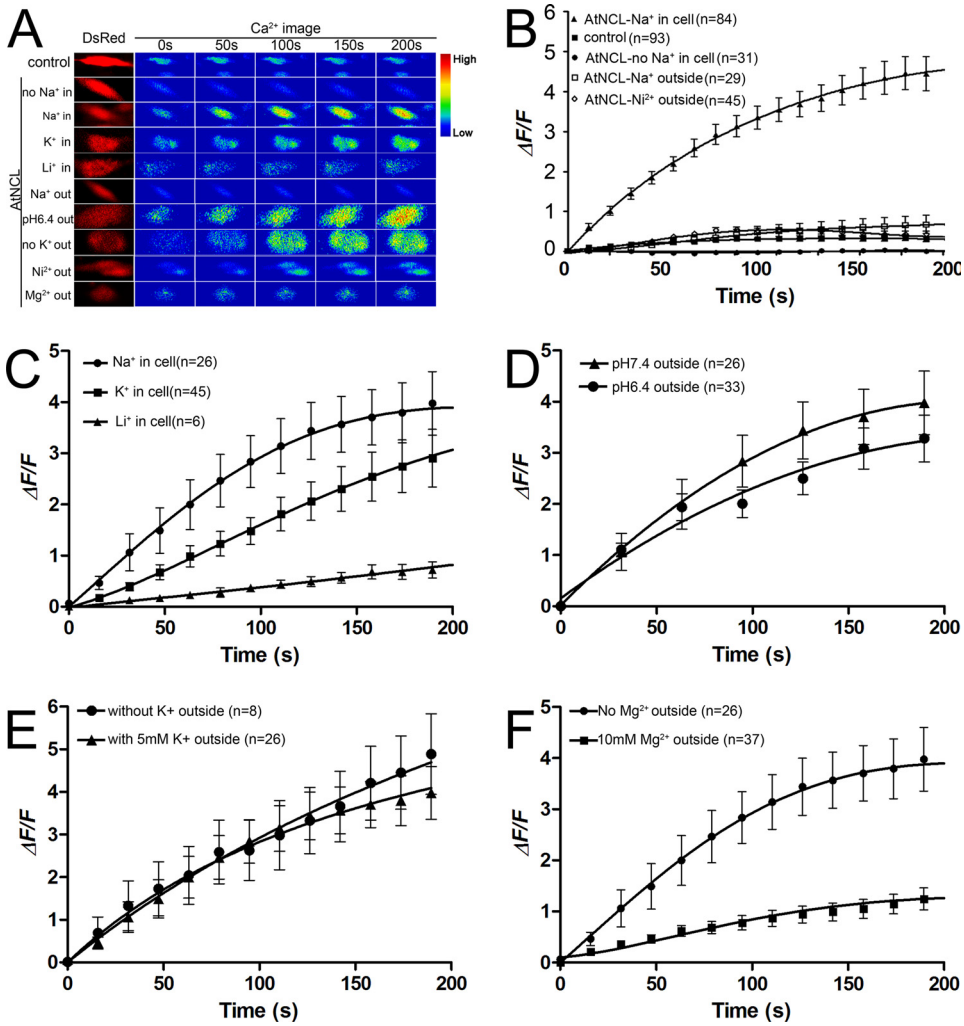

FIGURE 3. **Time course of Na^+ gradient-dependent Ca^{2+} transport in CHO-K1 cells expressing AtNCL.** *A*, pseudocolor images of CHO-K1 cells. The Ca^{2+} image was transformed from the Fluo-3 signal. *B–F*, statistical diagram of the CHO-K1 cells with treatments. The data shown are the mean values for the samples. *Bar*, the S.E. *B*, $[Ca^{2+}]_{cyt}$ level in the AtNCL-expressing cells increased. In comparison, the vector control and unloaded cells showed little change, whereas outside 5 mM Ni^{2+} or 150 mM Na^+ inhibited AtNCL activity. *C*, ion selectivity test of AtNCL. *D*, changing of outside pH from 7.4 to 6.4 having no effect on AtNCL-mediated Ca^{2+} uptake. *E*, outside K^+ not necessary for Ca^{2+} uptake. *F*, outside 10 mM Mg^{2+} inhibition Ca^{2+} uptake.

of the PCRs was determined by melt curve analysis of the amplified products using the standard methods installed in the system. The comparative ΔΔCT method was employed to evaluate relative quantities of each product amplified from the samples. All qRT-PCRs were performed in biological triplicates using RNA samples extracted from three independent plant materials grown under identical growth conditions.

β-Glucuronidase (GUS) Assay—Histochemical staining and fluorometric assays were performed according to the method reported by Jefferson (66).

Bacterial Recombinant Protein Expression and $^{45}Ca^{2+}$ Overlay Assays—The putative EF-hand Ca^{2+} binding domain (CaBD) sequence from AtNCL was cloned into pET-30(a) (Novagen) then transformed into *Escherichia coli* BL21 (DE3) cells (Novagen). His-tagged recombinant AtNCL was separated using Ni-affinity column (Novagen).The binding of $^{45}Ca^{2+}$ to CaBD of AtNCL was assayed as described (47). The purified protein was resolved on a 12 or 18% SDS-polyacrylamide gel then transferred to PVDF membrane and incubated for 30 min with 100 mCi/ml $^{45}CaC1_2$. The membrane was then washed and exposed to a storage PhosphorImage screen for 12 h. Images were collected using a Typhoon 9210 imager (Amersham Biosciences).

Measurement of Reverse-mode NCX Activity—Full-length *AtNCL* CDS with an extra Kozak sequence (GCCACC) before the initiation codon was cloned into pDsRed1-N1 using NdeI and AgeI. CHO-K1 cells were transfected with the resulting construct by electroporation as described (48). Reverse-mode NCX activity was measured as described (49). The fluorescence intensity was calculated at each time point before and after the addition of Ca^{2+} containing loading buffer (F_{basal} and F, respectively). The data for each cell were plotted as follows: $\Delta F/F = (F - F_{basal})/F_{basal}$.

Fluorescence Imaging—Fluorescence microscopy was performed using a Zeiss LSM 510 Meta microscope (Carl Zeiss Micro Imaging, Inc.). For yellow fluorescent protein (YFP) and propidium iodide (PI) imaging, an argon ion laser at 514 nm was used for excitation; emission was detected using a BP500–550 nm filter for YFP and LP615 nm for PI. Fluo-3 quantitative analysis was done as described (50, 51). Excitation of Fluo-3 was

performed using an argon ion laser at 488 nm. Emitted light was detected through a BP505-530-nm filter from a 545-nm dichroic mirror. DsRed fluorescence was excited using a green helium-neon laser at 543 nm and was detected through a 545-nm dichroic mirror and LP560-nm filter. The images were processed using LSM 4.2 software (Carl Zeiss Micro Imaging, Inc.).

Plant Membrane Fractionation and Western Blotting—Protein extracts were prepared from the wild-type or transgenic seedlings and separated into soluble and membrane fractions by ultracentrifugation as described previously (52). The fractions were then analyzed by Western blotting using anti-GFP serum as the primary antibody.

Element Analysis by AAS—The pretreated or untreated seedlings were washed with deionized water, dried using a blast dryer, and weighed. The seedlings were then subjected to digestion by the aqueous method using the chloric acid/perchloric acid (4:1, v/v) method. Next, the digested samples were diluted with deionized water and analyzed by AAS (AA240FS+240Z, Varian).

$[Ca^{2+}]_{cyt}$ Measurement Using Aequorin—atncl was crossed with a *p35S::Aequorin* transgenic line. The $[Ca^{2+}]_{cyt}$ level in the homozygotes was then determined as described (53).

Noninvasive Ion Flux Measurement Using an Ion-selective Microelectrode—The net fluxes of Ca^{2+} and H^+ in the root tips of 4-day-old seedlings grown on MS plates were measured noninvasively by SIET (54) using the BIO-001A SIET system (Xuyue (Beijing) Science and Technology Co., Ltd., Beijing, China). The SIET system measures static ionic/molecular concentrations and concentration gradients using ion-selective microelectrodes (55). The concentration gradient was measured by moving the electrode repeatedly between two positions along a predefined excursion (5–30 μm) at a fixed frequency in the range of 0.3–0.5 Hz.

RESULTS

AtNCL Is a Putative NCX—AtNCL (At1g53210) was predicted as a sodium/calcium exchanger family protein by the TAIR database. *AtNCL* comprises seven exons and six introns, encoding a putative protein with 585 amino acids. The N-terminal-most 22 amino acids in AtNCL comprise a putative signaling peptide (analyzed by SignalP). The protein had 10 putative transmembrane domains, with a hydrophilic loop between the fifth and sixth transmembrane domains containing two predicted EF-hand domains (analyzed by SMART). The deduced structure of AtNCL is similar to HsNCX1 from *Homo sapiens* (supplemental Fig. S1). AtNCL was considered a relative of CAXs (56), but it could not function as CAX in yeast, even if they have similar localization in yeast cells (Fig. 1). CAXs always have a conserved N-terminal autoinhibitory sequence (57–59); however, N-terminal deleted sAtNCL also cannot recover the yeast K667 phenotype (Fig. 1). On the other hand, AtNCL cannot work as a NHX in yeast (Fig. 1*C*), so we wanted to know whether it was a NCX-like protein.

Ca^{2+} Binding Ability of AtNCL—Because animal NCXs have intracellular loop with Ca^{2+} binding activity, we have tested the Ca^{2+} binding ability of AtNCL. Ca^{2+}-dependent electrophoretic mobility shift and $^{45}Ca^{2+}$ binding assays were used to

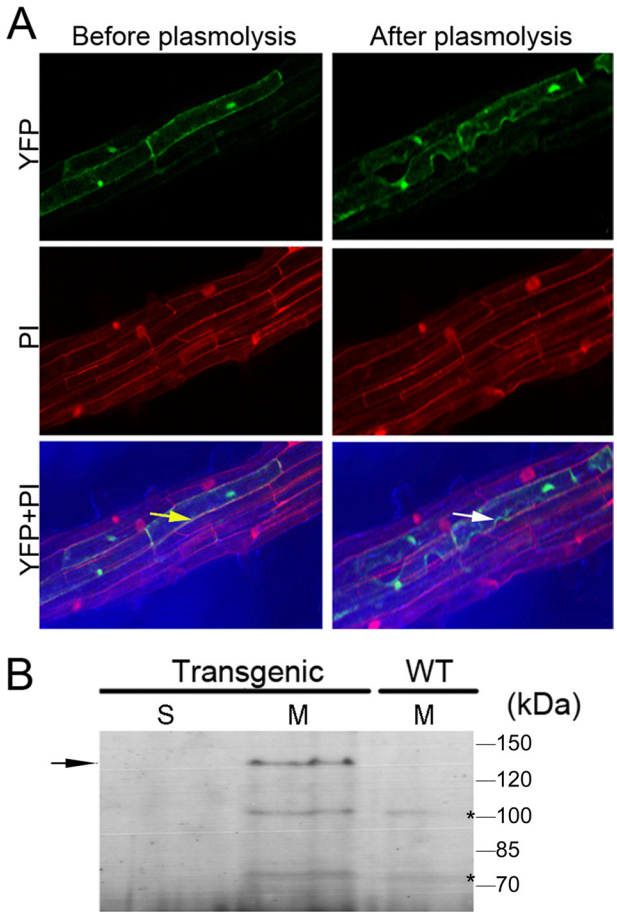

FIGURE 4. **The membrane localization of AtNCL in *Arabidopsis*.** *A*, laser-scanning confocal microscopy was used to determine the subcellular localization of an AtNCL-YFP fusion protein in transgenic root cells before and after plasmolysis with 30% sucrose. *YFP*, YFP channel; *PI*, PI channel; *YFP-PI*, merged image. The *yellow arrow* indicates the merged yellow signal from the cell membrane and cell wall, whereas the *white arrow* indicates the green color of the plasma membrane after plasmolysis. *B*, immunoblot analysis of various subcellular fractions with anti-GFP serum is shown. *Transgenic*, 3–4-week-old AtNCL-YFP-transgenic plants; *WT*, Col-0 seedlings; *S*, soluble protein; *M*, microsomal protein. The molecular masses of the standards are shown at the *right* of the sections. The AtNCL-YFP-specific band is indicated by an arrow on the *left*; the nonspecific bands are labeled by *asterisks*.

examine the predicted the Ca^{2+} binding ability of the putative EF-hand domain in AtNCL (amino acids 262–430; CaBD). The vector pET-30(a)-CaBD was constructed as shown in supplemental Table S1, and recombinant CaBD tagged with six His residues at its N terminus was expressed in *E. coli*. Before loading the sample, EGTA or divalent ions were added to the sample. By SDS-PAGE, CaBD ran faster in the presence of 5 mM Ca^{2+} than it did in the presence of EGTA or the bivalent ions Mg^{2+} and Mn^{2+} (Fig. 2*A*). According to our $^{45}Ca^{2+}$ binding assay results, recombinant CaBD bound Ca^{2+} as did our positive control, recombinant *Arabidopsis* CaM isoform 2 (AtCaM2), a known Ca^{2+}-binding protein, whereas our negative control, bovine serum albumin (BSA), did not (Fig. 2*B*).

AtNCL Possesses NCX-like Activity in CHO-K1 cells—To assess whether AtNCL has NCX-like activity, a CHO-K1 cell-based heterologous expression system was used. CHO-K1 cells transfected with pAtNCL-DsRed were tested against CHO-K1 cells transfected with pDsRed1-N1 as a control. The $[Ca^{2+}]_{cyt}$ was indicated by Fluo-3 fluorescence. In Na^+-free buffer con-

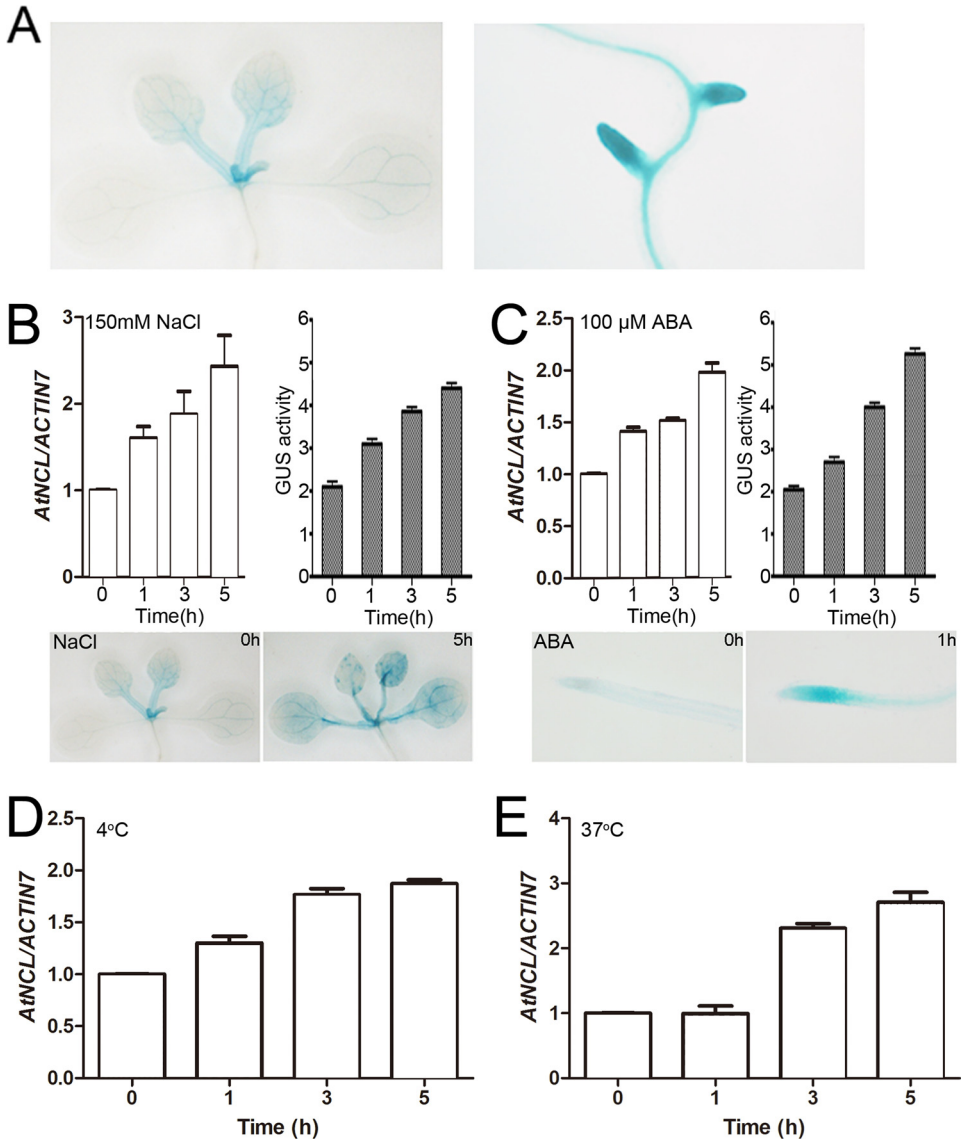

FIGURE 5. **AtNCL expression under normal conditions and in response to stress.** *A*, GUS staining of *AtNCL*::*AtNCL* cDNA-*GUS* transgenic seedlings under normal growth conditions. *B*, qRT-PCR and GUS assay of seedling exposure to 150 mM NaCl. *C*, qRT-PCR and GUS assay of seedling exposure to 100 μM ABA. *D*, qRT-PCR assay of wild-type seedling exposure to 4 °C. *E*, qRT-PCR assay of wild-type seedling exposure to 37 °C.

taining 2 mM Ca^{2+}, the signal from the Na^+-loaded AtNCL-expressing cells rose to saturation within 5 min whereas the vector control showed little signal (Fig. 3*B*). In contrast, the $[Ca^{2+}]_{cyt}$ did not increase significantly if the cells were not loaded with Na^+ (Fig. 3*B*). This suggests that the reverse NCX activity in the AtNCL-transfected cells (Fig. 3) was much higher than in the controls (Fig. 3). This activity was inhibited by 150 mM extracellular Na^+ (the concentration was set approximately equal to the inner Na^+ concentration to offset the Na^+ gradient) or by 5 mM Ni^{2+}, a NCX inhibitor used in animal cell (60) (Fig. 3*B*).

To confirm the ion selectivity for the exchange function of AtNCL, we performed another set of Ca^{2+} flux assays using cells loaded with a buffer solution containing Na^+, K^+, or Li^+. The result demonstrated that Na^+ and K^+ both can drive the Ca^{2+} flux and Na^+ is more efficient than K^+. However, Li^+ had no effect (Fig. 3*C*). Proton concentration was increased outside the cell by changing the bath buffer pH from 7.4 to 6.4, and the Na^+/Ca^{2+} exchange activity was not significantly affected (Fig. 3*D*).

To reveal whether the activity of AtNCL is dependent on K^+-like Na^+/Ca^{2+}-K^+ exchanger, we tested the bath buffer with K^+ or without K^+, respectively. The data indicated that outside K^+ was not necessary for AtNCL activity (Fig. 3*E*).

Mg^{2+} was reported not affect NCX activity (61). Here, we tested the Mg^{2+} effect on AtNCL, by add 10 mM Mg^{2+} to bath buffer. The result suggested that Mg^{2+} can suppress the AtNCL activity (Fig. 3*F*). Overall, AtNCL has NCX-like Ca^{2+} uptake activity in CHO-K1 cells.

Membrane Localization of AtNCL in Planta—AtNCL was reported to be localized to the vacuole by prediction and proteomics strategy (62–65). In this study, *p35S::AtNCL-YFP* was constructed and transformed into *Arabidopsis*, the signal in the AtNCL-YFP transgenic seedlings was stronger near the plasma membrane after plasmolysis (Fig. 4*A*). Overlap detected between the PI and YFP signals indicated that AtNCL may localized to the

plasma membrane in the transgenic root cells. However, AtNCL-YFP was also detected at the inner membrane.

Next, microsomal proteins were extracted from the *p35S::AtNCL-YFP* transgenic lines and probed with anti-GFP antibodies (Fig. 4*B*). A specific band was detected in microsome fraction but not in the soluble proteins from the transgenic lines or the microsomal proteins from wild-type seedlings.

AtNCL Expression in Arabidopsis—The expression pattern of *AtNCL* was examined using a GUS reporter gene fusion system (66). *pAtNCL::AtNCL-GUS* was constructed as described in supplemental Table S1 and transformed into *Arabidopsis*. GUS staining of 10 independent transgenic lines revealed that *AtNCL* was expressed broadly in the seedlings and flowers under normal growth conditions (Fig. 5*A*).

AtNCL expression was increased during abiotic stress, such as salt, ABA, heat shock, and cold stress, as indicated by qRT-PCR and GUS assay (Fig. 5, *B–E*). *AtNCL* expression increased within 1 h of exposure to 150 mM NaCl and reached its peak after approximately 5 h (Fig. 5*B*). Expression of the gene was unchanged following exposure to the same concentration of LiCl or in a mock sample under salt stress (data not shown). Exogenous ABA treatment caused a similar change in AtNCL expression (Fig. 5*C*). Heat shock and cold stress also increased AtNCL expression; however, heat shock had a greater effect than cold stress (Fig. 5, *D* and *E*).

Phenotypic Analysis of atncl Mutant and Overexpression Lines—The phenotypes of several *atncl* loss-of-function mutants and overexpression lines under salt stress were investigated (Fig. 6). Two *AtNCL* T-DNA insertion lines, *atncl-1* and *atncl-2*, were isolated from the SAIL collection. The T-DNA was inserted into the sixth and third introns of *AtNCL* in *atncl-1* and *atncl-2*, respectively. Full-length *AtNCL* mRNA was not detected in either of the mutant lines (Fig. 6, *A* and *B*). Both the *atncl-1* and *atncl-2* alleles were backcrossed with wild-type Col-0. BASTA resistance was observed among the F2 progeny at a 3:1 ratio, indicating that both alleles may contain a single T-DNA insertion with a functional selection marker. Next, *p35S::AtNCL-GUS* was transformed into *Arabidopsis* ecotype Col-0 and selected using Hygromycin B. *atnclox*, a single-copy insertion line, was included in the experiment.

No differences were detected in *atncl* and *atnclox* in terms of seed germination, plant growth, and flowering time under normal growth conditions compared with wild-type Col-0. However, under salt stress conditions, the *atncl* mutant seedlings were less sensitive than wild-type or the overexpression lines. The survival rate and chlorophyll contents were measured after treatment with 150 mM NaCl (Fig. 6*C*). The survival rate for *atncl-2* was 83.2% compared with 62.5 and 42.8% for wild-type and the overexpression lines, respectively (Fig. 6*C*). The average total chlorophyll content for *atncl-2* after salt stress was 0.308 mg/g fresh weight, compared with 0.261 and 0.246 mg/g fresh weight for wild-type and the overexpression lines, respectively (Fig. 6*C*), whereas the length of roots of *atncl-2* showed no difference with wild type and overexpression lines. The survival rate for *atncl-1* was similar to that for *atncl-2* (supplemental Fig. S4). The survival rate and chlorophyll contents of mutant seedlings were also slightly higher than wild type after heat shock and freezing stress (supplemental Fig. S5).

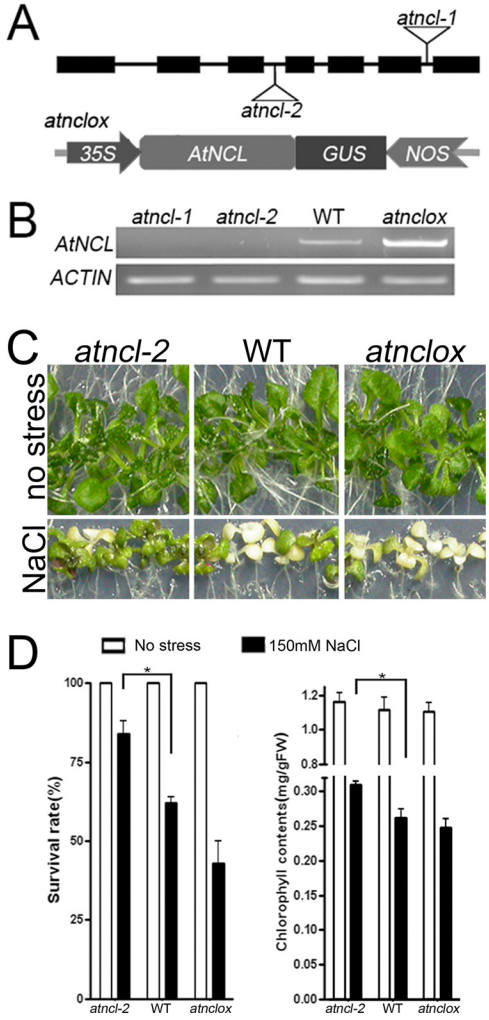

FIGURE 6. **Functional analysis of AtNCL in plant.** *A*, plant materials. The *upper panel* shows a diagram of *AtNCL* with *triangles* representing the sites of the T-DNA insertions in *atncl-1* and *-2*. The *lower panel* shows the construction of the overexpression vector. Full-length *AtNCL* cDNA was cloned into pCAMBIA1300 under control of the *CaMV* 35S-promoter with a NOS terminator and *GUS* as the reporter gene. *B*, RT-PCR analysis of total RNA extracted from the seedlings at 10 days after germination. *ACTIN7* was amplified as an internal control. *C*, growth phenotypes of seedlings grown on 1/2 MS containing 150 mM NaCl for 7 days beginning at 7 days after germination. *D*, survival rate and chlorophyll content after 7 days of salt stress. Seedlings without salt stress were used as a control. The test was performed at least three times using Prism 4 ($n = 30$). The columns show the mean value plus the S.E. (*error bars*). Those pairs for which $p < 0.05$ are marked with an *asterisk*.

atncl Mutants Show an Altered Ca Content and Ca^{2+} Flux Activity during Salt Stress—AAS was used to verify the total elemental Na and Ca contents in plants with or without NaCl stress (Fig. 7*A*). Under normal growth conditions, the total Na content in the *atncl* mutant seedlings was slightly lower than that in the wild-type or *atnclox* seedlings, whereas the level of Ca was higher. The ion content change in the *atnclox* lines was opposite that in the mutant lines. Under conditions of NaCl stress, the Na and Ca content change was different (Fig. 7*A*). The Ca content in the *atncl* loss-of-function mutants was largely unchanged, whereas that in wild-type and the overexpression lines was decreased. In comparison, the Na content in wild-type and the overexpression lines was much higher than that in *atncl*.

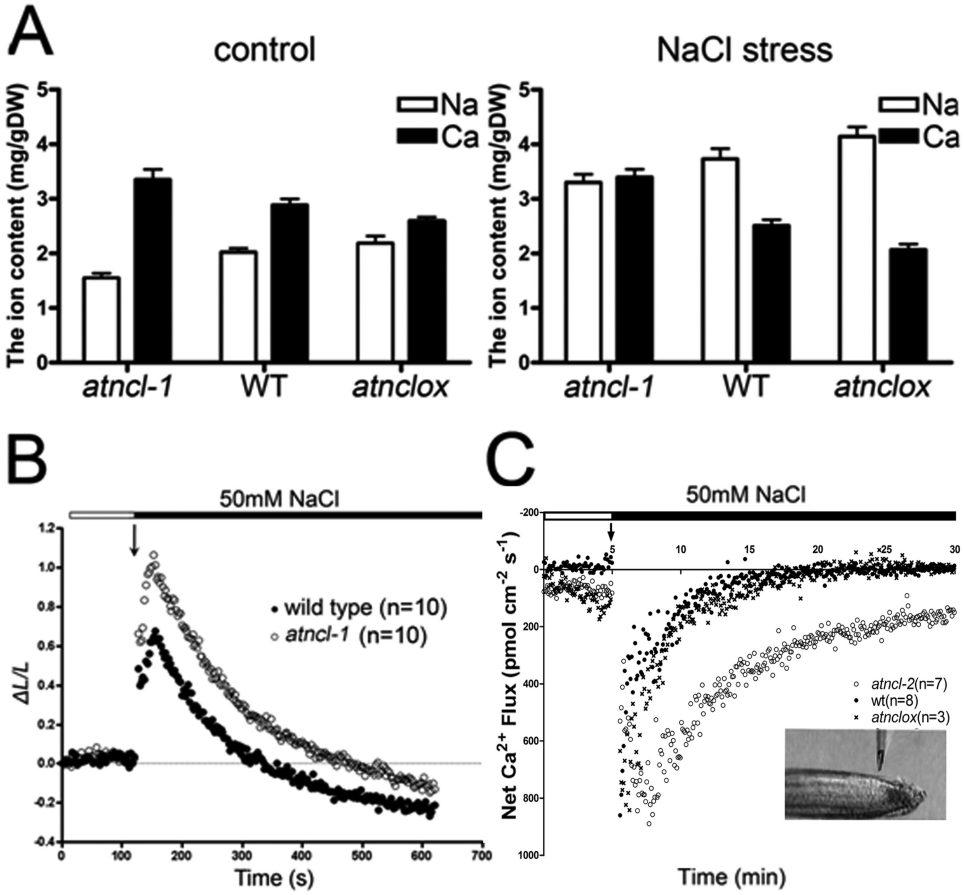

FIGURE 7. **AtNCL participates in Na^+ and Ca^{2+} ion homeostasis.** *A*, seedlings treated with or without 200 mM NaCl for 1 h were subjected to AAS. The experiment was repeated at least three times. The columns show the mean value plus the S.E. (*error bars*). *B*, kinetics of the $[Ca^{2+}]_{cyt}$ level in the seedlings at 4 days after germination was determined using transgenic aequorin. *C*, Ca^{2+} flux in the roots was measured by SIET. The bath $[Ca^{2+}]$ was 0.1 mM. After approximately 5 min at the resting level, 50 mM NaCl was added. The Ca^{2+} flux was then measured for about 30 min in the root tips (shown in the *inset*). The number of samples is shown in *parentheses*. The data in *B* and *C* are the mean values for the samples.

Transgenic *p35S::aequorin* seedlings were used to monitor the $[Ca^{2+}]_{cyt}$ in response to salt stress (Fig. 7*B*). Aequorin luminescence in the *atncl* and wild-type seedlings quickly increased approximately 2-fold following exposure to 50 mM NaCl. However, *atncl* showed stronger luminescence than wild type during their return to the resting level, which took about 600 s. This indicates that the $[Ca^{2+}]_{cyt}$ is higher in the *atncl* seedlings compared with the wild-type seedlings.

To determine whether AtNCL participates in Na^+/Ca^{2+} transport, SIET was used to monitor the flux of Ca^{2+} at the root tip during salt stress (Fig. 7*C*). After the addition of 50 mM NaCl to the test system, an outward Ca^{2+} flux exceeding 800 pmol·cm^{-2} s^{-1} was recorded in wild-type seedlings, *atncl* and *atnclox*. The Ca^{2+} flux reached the resting level within 10 min in wild type and *atnclox*, whereas in the *atncl* mutant seedlings, the flux lasted for approximately 30 min before returning to the resting level. In comparison, the H^+ flux patterns in *atncl* and wild type were similar following treatment with 50 mM NaCl (supplemental Fig. S6). The H^+ flux increased rapidly, reaching its peak within 5 min; thereafter, the flux decreased gradually, returning to the resting level within 20 min.

DISCUSSION

AtNCL May be a Novel Exchanger in Plant—AtNCL was once predicted to be a CAX-like protein (56); however AtNCL cannot work like CAXs in yeast to suppress the Ca^{2+}-hypersensitive phenotype in K667, even if they share similar localization in yeast (Fig. 1). The *AtNCL*-transformed yeast growth was not affected by moderate change in pH (supplemental Fig. S3). By increasing the outside H^+, the Ca^{2+} uptake of *AtNCL*-expressing cells was not affected. *AtNCL* also cannot work as a NHX in yeast (Fig. 1*C*), and AtNCL showed NCX-like activity in CHO-K1 cells (Fig. 3). By SIET, H^+ flux patterns in *atncl* and wild type were similar during salt stress. These data suggested that AtNCL was probably a NCX-like protein rather than a CAX.

Recently, the structure of a NCX family member NCX_Mj had been resolved (27), and some critical site for ion binding and transport was identified. Sequence alignment analysis of NCXs and AtNCL showed that some critical amino acids that were conserved in NCXs also could be found in AtNCL, such as in α1 and α2 repeat, conservative glutamic acid or aspartic acid for bidentate Ca^{2+} coordination, conservative serine or threonine for extracellular Na^+ binding site, and some Thr, Ser, or asparagine sites forming the Na^+ site on the intracellular side were also found in AtNCL (supplemental Fig. S2). This suggests that AtNCL may share a similar ion exchange mechanism with NCXs.

However, there were also some differences between AtNCL and mammalian NCXs. For instance, unlike the NCXs (27,61), the Ca^{2+} uptake activity of AtNCL can be driven by the K^+

gradient and inhibited by Mg^{2+} (Fig. 3), but outside K^+ was not necessary for the Ca^{2+} uptake (Fig. 3). This suggested that AtNCL might not be a Na^+/Ca^{2+}-K^+ exchanger-like protein.

AtNCL May Contribute to Ca^{2+} Homeostasis under Abiotic Stress—The results of a previous microarray analysis and expression level analysis indicate that salt stress, heat shock, cold stress, and ABA treatment can induce AtNCL expression (Fig. 5). In addition, it is known that Ca^{2+} signaling can be evoked by various stimuli. We found that salt and ABA stress induced greater *AtNCL* expression than temperature stimuli; however, we focused on the salt stress phenotype in our subsequent experiments to determine the function of AtNCL in plants. *AtNCL* was expressed broadly in *Arabidopsis* seedlings, flowers, and root tips (Fig. 5). Measurement of the elemental Ca content by AAS showed that under normal conditions, the *atncl*, wild-type, and overexpression seedlings all maintained a balance between Ca^{2+} and Na^+ (Fig. 7*A*), whereas during salt stress the Ca^{2+} signal was ended by transfer of the Ca^{2+} from the cytoplasm to the apoplast or vacuole. During this process, AtNCL may be activated to extrude Ca^{2+}; thus, *atncl* showed a higher $[Ca^{2+}]_{cyt}$ and root surface Ca^{2+} flux by SIET than wild type (Fig. 7*C*). The enhanced Ca^{2+} signal may evoke a stronger response to salt stress, which may explain the improved growth of the *atncl* mutant lines compared with wild-type or the overexpression lines under conditions of salt stress.

To better understand the role of AtNCL, aequorin was used to monitor the $[Ca^{2+}]_{cyt}$ level. We found that during salt stress, the *atncl* seedlings had higher $[Ca^{2+}]_{cyt}$ than wild type. This apparent defect in Ca^{2+} extrusion was likely caused by the lack of AtNCL. Measurement of the root surface ion flux by SIET revealed a slower Ca^{2+} flux recovery process in the *atncl* mutant seedlings, which might be a consequence of the slower recovery of the $[Ca^{2+}]_{cyt}$.

It has been shown that the root surface ion flux might originate from ion exchange at the cell wall (67); however, the manner of the ion flux differed between the *atncl* and wild-type seedlings (Fig. 7*C*), possibly due to the difference in ion transport activity. In some cases, the detected ion flux might reflect a combination of ion transport across the cell wall and membrane. Even if AtNCL is absent, there are other transporters capable of terminating the Ca^{2+} signal, such as CAXs or Ca^{2+} pumps in the endomembrane and plasma membrane. Thus, the mutant seedlings showed no difference from wild type under normal conditions. AtNCL may behave like an animal NCX (68), regulating Ca^{2+} homeostasis under abnormal conditions. However, further experiments are needed to clarify how many Na^+ ions AtNCL exchanges for one Ca^{2+} and the regulating mechanism of its exchanger activity *in planta.*

Acknowledgments—We thank Dr. M. R. Knight for the p35S:: Aequorin transgenic Arabidopsis seeds, Dr. K. Cunningham and Dr. Baoshan Wang for the yeast strain and vector used for CAX complementation, Dr. José M. Pardo for the yeast strain and vector for NHX complementation, Dr. L. S. Kao for assistance during the NCX activity tests, Dr. Ying Sun and Ligeng Ma for helpful discussions, Junfeng Zhao for technical assistance with the laser scanning microscopy, and the Arabidopsis Biological Resource Center for the T-DNA insertion lines.

REFERENCES

1. Spalding, E. P., and Harper, J. F. (2011) The ins and outs of cellular Ca^{2+} transport. *Curr. Opin. Plant Biol.* **14,** 715–720
2. Poovaiah, B. W., and Reddy, A. S. (1993) Calcium and signal transduction in plants. *Crit. Rev. Plant Sci.* **12,** 185–211
3. Monroy, A. F., and Dhindsa, R. S. (1995) Low-temperature signal transduction: induction of cold acclimation-specific genes of alfalfa by calcium at 25 °C. *Plant Cell* **7,** 321–331
4. Knight, H., Trewavas, A. J., and Knight, M. R. (1997) Calcium signalling in *Arabidopsis thaliana* responding to drought and salinity. *Plant J.* **12,** 1067–1078
5. Knight, H., Trewavas, A. J., and Knight, M. R. (1996) Cold calcium signaling in *Arabidopsis* involves two cellular pools and a change in calcium signature after acclimation. *Plant Cell* **8,** 489–503
6. Knight, H., Brandt, S., and Knight, M. R. (1998) A history of stress alters drought calcium signalling pathways in *Arabidopsis*. *Plant J.* **16,** 681–687
7. Dodd, A. N., Kudla, J., and Sanders, D. (2010) The language of calcium signaling. *Annu. Rev. Plant Biol.* **61,** 593–620
8. Bush, D. S. (1995) Calcium regulation in plant cells and its role in signaling. *Plant Mol. Biol.* **46,** 95–122
9. Paredes-Gamero, E. J., Barbosa, C. M., and Ferreira, A. T. (2012) Calcium signaling as a regulator of hematopoiesis. *Front. Biosci.* **4,** 1375–1384
10. Baczyk, D., Kingdom, J. C., and Uhlén, P. (2011) Calcium signaling in placenta. *Cell Calcium* **49,** 350–356
11. Baba, Y., and Kurosaki, T. (2011) Impact of Ca^{2+} signaling on B cell function. *Trends Immunol.* **32,** 589–594
12. Sanders, D., Brownlee, C., and Harper, J. F. (1999) Communicating with calcium. *Plant Cell* **11,** 691–706
13. Piñeros, M., and Tester, M. (1997) Calcium channels in higher plant cells: selectivity, regulation and pharmacology. *J. Exp. Bot.* **48,** 551–577
14. Axelsen, K. B., and Palmgren, M. G. (2001) Inventory of the superfamily of P-type ion pumps in *Arabidopsis*. *Plant Physiol.* **126,** 696–706
15. Axelsen, K. B., and Palmgren, M. G. (1998) Evolution of substrate specificities in the P-type ATPase superfamily. *J. Mol. Evol.* **46,** 84–101
16. Briskin, D. P. (1990) Ca^{2+}-translocating ATPase of the plant plasma membrane. *Plant Physiol.* **94,** 397–400
17. Ferrol, N., and Bennett, A. B. (1996) A single gene may encode differentially localized Ca^{2+}-ATPases in tomato. *Plant Cell* **8,** 1159–1169
18. Pfeiffer, W., and Hager, A. (1993) A Ca^{2+}-ATPase and a Mg^{2+}/H^+-antiporter are present on tonoplast membranes from roots of *Zea mays* L. *Planta* **191,** 377–385
19. Hong, B., Ichida, A., Wang, Y., Gens, J. S., Pickard, B. G., and Harper, J. F. (1999) Identification of a calmodulin-regulated Ca^{2+}-ATPase in the endoplasmic reticulum. *Plant Physiol.* **119,** 1165–1176
20. Reuter, H., and Seitz, N. (1968) The dependence of calcium efflux from cardiac muscle on temperature and external ion composition. *J. Physiol.* **195,** 451–470
21. Nicoll, D. A., Longoni, S., and Philipson, K. D. (1990) Molecular cloning and functional expression of the cardiac sarcolemmal Na^+-Ca^{2+} exchanger. *Science* **250,** 562–565
22. Nakasaki, Y., Iwamoto, T., Hanada, H., Imagawa, T., and Shigekawa, M. (1993) Cloning of the rat aortic smooth muscle Na^+/Ca^{2+} exchanger and tissue-specific expression of isoforms. *J. Biochem.* **114,** 528–534
23. Tsuruya, Y., Bersohn, M. M., Li, Z., Nicoll, D. A., and Philipson, K. D. (1994) Molecular cloning and functional expression of the guinea pig cardiac Na^+-Ca^{2+} exchanger. *Biochim. Biophys. Acta* **1196,** 97–99
24. Ruknudin, A., Valdivia, C., Kofuji, P., Lederer, W. J., and Schulze, D. H. (1997) Na^+/Ca^{2+} exchanger in *Drosophila*: cloning, expression, and transport differences. *Am. J. Physiol.* **273,** C257–265
25. He, Z., Tong, Q., Quednau, B. D., Philipson, K. D., and Hilgemann, D. W. (1998) Cloning, expression, and characterization of the squid Na^+–Ca^{2+} exchanger (NCX-SQ1). *J. Gen. Physiol.* **111,** 857–873
26. Marshall, C. R., Pan, T. C., Le, H. D., Omelchenko, A., Hwang, P. P., Hryshko, L. V., and Tibbits, G. F. (2005) cDNA cloning and expression of the cardiac Na^+/Ca^{2+} exchanger from Mozambique tilapia (*Oreochromis mossambicus*) reveal a teleost membrane transporter with mammalian temperature dependence. *J. Biol. Chem.* **280,** 28903–28911

27. Liao, J., Li, H., Zeng, W., Sauer, D. B., Belmares, R., and Jiang, Y. (2012) Structural insight into the ion-exchange mechanism of the sodium/calcium exchanger. *Science* **335,** 686–690
28. Nicoll, D. A., Ottolia, M., Lu, L., Lu, Y., and Philipson, K. D. (1999) A new topological model of the cardiac sarcolemmal Na^+-Ca^{2+} exchanger. *J. Biol. Chem.* **274,** 910–917
29. Nicoll, D. A., Hryshko, L. V., Matsuoka, S., Frank, J. S., and Philipson, K. D. (1996) Mutation of amino acid residues in the putative transmembrane segments of the cardiac sarcolemmal Na^+-Ca^{2+} exchanger. *J. Biol. Chem.* **271,** 13385–13391
30. Levitsky, D. O., Nicoll, D. A., and Philipson, K. D. (1994) Identification of the high affinity Ca^{2+}-binding domain of the cardiac Na^+-Ca^{2+} exchanger. *J. Biol. Chem.* **269,** 22847–22852
31. Philipson, K. D., and Nicoll, D. A. (2000) Sodium-calcium exchange: a molecular perspective. *Annu. Rev. Physiol.* **62,** 111–133
32. Blaustein, M. P., and Lederer, W. J. (1999) Sodium/calcium exchange: its physiological implications. *Physiol. Rev.* **79,** 763–854
33. Weber, C. R., Piacentino, V., 3rd, Ginsburg, K. S., Houser, S. R., and Bers, D. M. (2002) Na^+-Ca^{2+} exchange current and submembrane [Ca^{2+}] during the cardiac action potential. *Circ. Res.* **90,** 182–189
34. Manohar, M., Shigaki, T., and Hirschi, K. D. (2011) Plant cation/H^+ exchangers (CAXs): biological functions and genetic manipulations. *Plant Biol.* **13,** 561–569
35. Zhao, J., Connorton, J. M., Guo, Y., Li, X., Shigaki, T., Hirschi, K. D., and Pittman, J. K. (2009) Functional studies of split *Arabidopsis* Ca^{2+}/H^+ exchangers. *J. Biol. Chem.* **284,** 34075–34083
36. Hirschi, K. D., Zhen, R. G., Cunningham, K. W., Rea, P. A., and Fink, G. R. (1996) CAX1, an H^+/Ca^{2+} antiporter from *Arabidopsis*. *Proc. Natl. Acad. Sci. U.S.A.* **93,** 8782–8786
37. Huang, L., Berkelman, T., Franklin, A. E., and Hoffman, N. E. (1993) Characterization of a gene encoding a Ca^{2+}-ATPase-like protein in the plastid envelope. *Proc. Natl. Acad. Sci. U.S.A.* **90,** 10066–10070
38. Yin, D., Kuczera, K., and Squier, T. C. (2000) The sensitivity of carboxyl-terminal methionines in calmodulin isoforms to oxidation by H_2O_2 modulates the ability to activate the plasma membrane Ca-ATPase. *Chem. Res. Toxicol.* **13,** 103–110
39. Pittman, J. K. (2011) Vacuolar Ca^{2+} uptake. *Cell Calcium* **50,** 139–146
40. Kronzucker, H. J., and Britto, D. T. (2011) Sodium transport in plants: a critical review. *New Phytol.* **189,** 54–81
41. Rodríguez-Rosales, M. P., Gálvez, F. J., Huertas, R., Aranda, M. N., Baghour, M., Cagnac, O., and Venema, K. (2009) Plant NHX cation/proton antiporters. *Plant Signal. Behav.* **4,** 265–276
42. Wang, Y. Z., Li, R. L., Xu, X. Z., and Zhu, W. C. (1994) Ca^{2+} transport across the tonoplast of wheat roots. *J. Wuhan Univ.* (*Nat. Sci. Ed*) (in Chinese) **5,** 111–115
43. Arnon, D. I. (1949) Copper enzymes in isolated chloroplasts: polyphenoloxidase in *Beta vulgaris*. *Plant Physiol.* **24,** 1–15
44. Xin, Z., and Browse, J. (1998) Eskimo1 mutants of *Arabidopsis* are constitutively freezing-tolerant. *Proc. Natl. Acad. Sci. U.S.A.* **95,** 7799–7804
45. Zheng, S. Z., Liu, Y. L., Li, B., Shang, Z. L., Zhou, R. G., and Sun, D. Y. (2012) Phosphoinositide-specific phospholipase C9 is involved in the thermotolerance of *Arabidopsis*. *Plant J.* **69,** 689–700
46. Quintero, F. J., Blatt, M. R., and Pardo, J. M. (2000) Functional conservation between yeast and plant endosomal Na^+/H^+ antiporters. *FEBS Lett.* **471,** 224–228
47. Maruyama, K., Mikawa, T., and Ebashi, S. (1984) Detection of calcium binding proteins by 45Ca autoradiography on nitrocellulose membrane after sodium dodecyl sulfate gel electrophoresis. *J. Biochem.* **95,** 511–519
48. Sambrook, J., and Russell, D. W. (2006) *The Condensed Protocols from Molecular Cloning: A Laboratory Manual*, pp. 599–621, Cold Spring Harbor Laboratory, Cold Spring Harbor, NY
49. Yang, Y. C., Fann, M. J., Chang, W. H., Tai, L. H., Jiang, J. H., and Kao, L. S. (2010) Regulation of sodium-calcium exchanger activity by creatine kinase under energy-compromised conditions. *J. Biol. Chem.* **285,** 28275–28285
50. Srikanth, S., Banerjee, S., and Hasan, G. (2006) Ectopic expression of a *Drosophila* $InsP_3R$ channel mutant has dominant-negative effects *in vivo*. *Cell Calcium* **39,** 187–196
51. Calderón-Sánchez, E. M., Ruiz-Hurtado, G., Smani, T., Delgado, C., Benitah, J. P., Gómez, A. M., and Ordóñez, A. (2011) Cardioprotective action of urocortin in postconditioning involves recovery of intracellular calcium handling. *Cell Calcium* **50,** 84–90
52. Tang, W., Deng, Z., Oses-Prieto, J. A., Suzuki, N., Zhu, S., Zhang, X., Burlingame, A. L., and Wang, Z. Y. (2008) Proteomics studies of brassinosteroid signal transduction using prefractionation and two-dimensional DIGE. *Mol. Cell Proteomics* **7,** 728–738
53. Knight, M. R., Campbell, A. K., Smith, S. M., and Trewavas, A. J. (1991) Transgenic plant aequorin reports the effects of touch and cold-shock and elicitors on cytoplasmic calcium. *Nature* **352,** 524–526
54. Vincent, P., Chua, M., Nogue, F., Fairbrother, A., Mekeel, H., Xu, Y., Allen, N., Bibikova, T. N., Gilroy, S., and Bankaitis, V. A. (2005) A Sec14p-nodulin domain phosphatidylinositol transfer protein polarizes membrane growth of *Arabidopsis thaliana* root hairs. *J. Cell Biol.* **168,** 801–812
55. Kühtreiber, W. M., and Jaffe, L. F. (1990) Detection of extracellular calcium gradients with a calcium-specific vibrating electrode. *J. Cell Biol.* **110,** 1565–1573
56. Shigaki, T., Rees, I., Nakhleh, L., and Hirschi, K. D. (2006) Identification of three distinct phylogenetic groups of CAX cation/proton antiporters. *J. Mol. Evol.* **63,** 815–825
57. Pittman, J. K., Sreevidya, C. S., Shigaki, T., Ueoka-Nakanishi, H., and Hirschi, K. D. (2002) Distinct N-terminal regulatory domains of Ca^{2+}/H^+ antiporters. *Plant Physiol.* **130,** 1054–1062
58. Pittman, J. K., Shigaki, T., Cheng, N. H., and Hirschi, K. D. (2002) Mechanism of N-terminal autoinhibition in the *Arabidopsis* Ca^{2+}/H^+ antiporter CAX1. *J. Biol. Chem.* **277,** 26452–26459
59. Pittman, J. K., and Hirschi, K. D. (2001) Regulation of CAX1, an *Arabidopsis* Ca^{2+}/H^+ antiporter: identification of an N-terminal autoinhibitory domain. *Plant Physiol.* **127,** 1020–1029
60. Kimura, J., Miyamae, S., and Noma, A. (1987) Identification of sodium-calcium exchange current in single ventricular cells of guinea pig. *J. Physiol.* **384,** 199–222
61. Kimura, J. (1996) Effects of external Mg^{2+} on the Na-Ca exchange current in guinea pig cardiac myocytes. *Ann. N.Y. Acad. Sci.* **779,** 515–520
62. Mitra, S. K., Gantt, J. A., Ruby, J. F., Clouse, S. D., and Goshe, M. B. (2007) Membrane proteomic analysis of *Arabidopsis thaliana* using alternative solubilization techniques. *J. Proteome Res.* **6,** 1933–1950
63. Dunkley, T. P., Hester, S., Shadforth, I. P., Runions, J., Weimar, T., Hanton, S. L., Griffin, J. L., Bessant, C., Brandizzi, F., Hawes, C., Watson, R. B., Dupree, P., and Lilley, K. S. (2006) Mapping the *Arabidopsis* organelle proteome. *Proc. Natl. Acad. Sci. U.S.A.* **103,** 6518–6523
64. Szponarski, W., Sommerer, N., Boyer, J. C., Rossignol, M., and Gibrat, R. (2004) Large-scale characterization of integral proteins from *Arabidopsis* vacuolar membrane by two-dimensional liquid chromatography. *Proteomics* **4,** 397–406
65. Carter, C., Pan, S., Zouhar, J., Avila, E. L., Girke, T., and Raikhel, N. V. (2004) The vegetative vacuole proteome of *Arabidopsis thaliana* reveals predicted and unexpected proteins. *Plant Cell* **16,** 3285–3303
66. Jefferson, R. (1987) Assaying chimeric genes in plants: the GUS gene fusion system. *Plant Mol. Biol. Rep.* **5,** 387–405
67. Shabala, S., and Newman, I. (2000) Salinity effects on the activity of plasma membrane H^+ and Ca^{2+} transporters in bean leaf mesophyll: masking role of the cell wall. *Ann. Bot.* **85,** 681–686
68. Eisner, D. A., and Sipido, K. R. (2004) Sodium calcium exchange in the heart: necessity or luxury? *Circ. Res.* **95,** 549–551